doi:10.1016/j.jmb.2007.12.049 J. Mol. Biol. (2008) 376, 1320–1333

JMB

Available online at www.sciencedirect.com

ScienceDirect

ELSEVIER

Yeast Rvb1 and Rvb2 are ATP-Dependent DNA Helicases that Form a Heterohexameric Complex

Anna Gribun[1]†, Kevin L. Y. Cheung[2]†, Jennifer Huen[1]†, Joaquin Ortega[2] and Walid A. Houry[1]*

[1]*Department of Biochemistry, University of Toronto, Toronto, ON, Canada M5S 1A8*

[2]*Department of Biochemistry and Biomedical Sciences, McMaster University, Hamilton, ON, Canada L8N 3Z5*

Received 26 October 2007; received in revised form 17 December 2007; accepted 19 December 2007
Available online 3 January 2008

Rvb1 and Rvb2 are highly conserved proteins present in archaea and eukaryotes. These proteins are members of a large superfamily of ATPases associated with diverse cellular activities—the AAA$^+$ superfamily. The Rvbs have been found in multiprotein complexes that have wide ranges of functions, including DNA repair, transcription, chromatin remodeling, ribosomal RNA processing, and small nucleolar RNA accumulation. Here we show that yeast Rvb1 and Rvb2 form a heterohexameric ring structure rather than the double-hexameric ring structure proposed to be formed by the human proteins. The yeast Rvb1/2 complex has enhanced ATPase activity compared with the individual Rvb proteins; furthermore, the ATPase activity of the Rvb1/2 complex is further increased in the presence of double-stranded DNA with 5′ or 3′ overhangs. The yeast Rvb1/2 ring undergoes nucleotide-dependent conformational changes as observed by electron microscopy. In addition, consistent with a role for these proteins in chromatin remodeling and DNA repair, the yeast Rvb1/2 complex exhibits DNA helicase activity with a preference for unwinding in the 5′-to-3′ direction. The individual Rvb proteins also exhibit helicase activity, albeit weaker than that of the Rvb1/2 complex. These results clearly establish the yeast Rvb1/2 complex as a heterohexameric ATP-dependent DNA helicase and highlight the possible roles played by the Rvb proteins within multiprotein complexes.

Edited by K. Morikawa

Keywords: AAA$^+$; electron microscopy; helicase; Rvb1; Rvb2

Introduction

Rvb1 and Rvb2 are two homologous and highly conserved protein members of the ATPases associated with diverse cellular *a*ctivities (AAA$^+$) superfamily. These proteins are present in archaea and in all eukaryotic genomes examined.[1] They are essential in yeast and *Drosophila melanogaster* and are likely to be essential in mammalian cells as well.[2–4] Rvb1 and Rvb2 are involved in many cellular processes. This is reflected in the multiplicity of names by which Rvb1 and Rvb2 proteins are known. Rvb1 (YDR190C in yeast) is also known as RuvBL1, Tip49a, Tip48/Tip49, ECP-54, Pontin, Tih1, p50, and Tap54β, while Rvb2 (YPL235W in yeast) is also known as RuvBL1, Tip49b, ECP-51, Tip49/Tip48, Reptin, Tih2, p47, and Tap54α.

Although the yeast Rvb proteins have no significant sequence similarity with the bacterial RuvB ATPase that promotes the branch migration and resolution of Holliday junctions in complex with RuvA and RuvC,[5–7] overexpression of bacterial RuvAB complex in yeast can complement *rvb1*Δ and *rvb2*Δ deletions.[8] Yeast Rvb1 and Rvb2 have been shown to affect the transcription regulation of 5% of yeast genes[9,10] and proposed to act as DNA helicases. Furthermore, they are implicated in a wide range of cellular activities, including DNA replication and repair,[2] cell cycle progression,[11] and chromatin remodeling.[9] More specifically, in mammalian cells, the Rvb proteins were found to

*Corresponding author. E-mail address: walid.houry@utoronto.ca.

† A.G., K.L.Y.C. and J.H. contributed equally to this work.

Abbreviations used: AAA$^+$, ATPases associated with diverse cellular *a*ctivities; dsDNA, double-stranded DNA; ssDNA, single-stranded DNA; TEM, transmission electron microscopy; STEM, scanning transmission electron microscopy; TMV, tobacco mosaic virus; M/L, mass per length.

modulate cellular transformation, signaling, apoptosis, and response to DNA damage by interacting with proteins such as β-catenin, c-Myc, and ATF2.[4,12] In addition, consistent with previous reports that implicate the Rvb proteins in modulating ribosomal RNA processing and small nucleolar RNA maturation,[13,14] we recently identified a new complex formed by Rvb1, Rvb2, Tah1, and Pih1 proteins, which we termed the R2TP complex,[15] that is involved in small nucleolar RNA accumulation (paper accepted in Journal of Cell Biology).

Although Rvb1 and Rvb2 might function independently, they probably function as a complex as shown *in vitro*[16] and *in vivo*.[11] In fact, it has been found that both Rvb1 and Rvb2 proteins are integral subunits of multiprotein complexes such as the chromatin remodeling INO80[17,18] and SWR-C[19–21] complexes, the histone acetylase Tip60 complex,[22] and the transcription activator c-Myc complex.[23] In all of these multiprotein complexes, the presence of Rvb1 and that of Rvb2 proteins were reported to be essential for their proper function.

The human Rvb1/2 complex has been imaged by electron microscopy and was found to consist of two stacked hexameric rings.[16] The crystal structure of human Rvb1 has been solved as a hexamer,[24] and the human Rvb1 sequence shares 69% sequence identity and 83% sequence similarity with yeast Rvb1 (Fig. 1). Based on that structure, the Rvb sequence can be divided into three structural fragments (Fig. 1): (1) an N-terminal discontinuous αβα subdomain of the AAA$^+$ domain, (2) an insertion domain within the αβα subdomain, and (3) a C-terminal all-α subdomain of the AAA$^+$ domain (Fig. 1). The insertion domain has been proposed to be a novel DNA/RNA binding domain.[24]

Reports on the *in vitro* ATPase and helicase activities of purified mammalian Rvbs have been rather controversial, with different groups reporting contradictory results. Some of these results indicate that rat Rvb1 alone and human Rvb2 alone are active ATPases and helicases.[3,28] However, the human Rvb1/2 complex was shown to have ATPase activity but lacked helicase activity.[16] Other groups were unable to detect ATPase or helicase activities for human Rvb1.[2,24]

As part of an effort aimed at understanding the function of the R2TP complex,[15] we endeavored to biochemically, biophysically, and structurally describe the yeast Rvb1 and Rvb2 proteins, both of

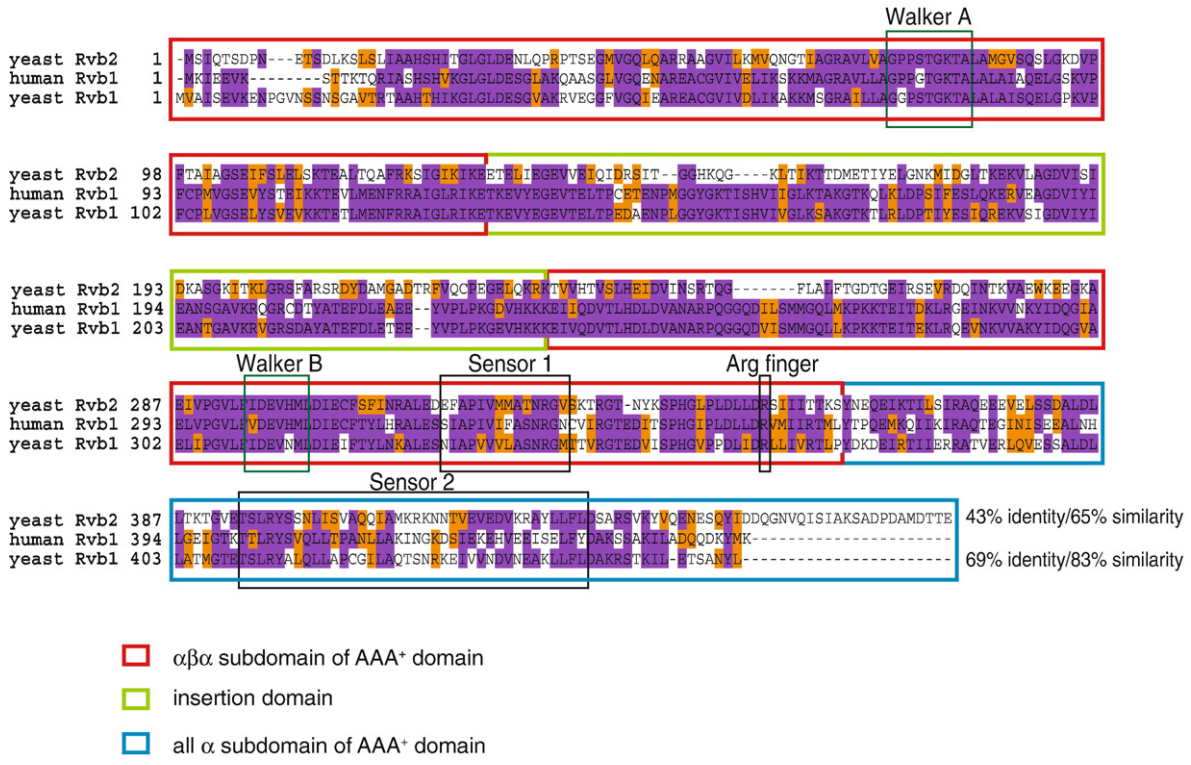

Fig. 1. Sequence alignment of yeast Rvb1 and Rvb2 with human Rvb1. Sequences of yeast Rvb1 (NP_010476), yeast Rvb2 (NP_015089), and human Rvb1 (NP_003698) were aligned using the multiple sequence alignment tool MUSCLE.[25,26] Similar and identical residues were colored using the online server BOXSHADE 3.21 [http://www.ch.embnet.org/software/BOX_form.html}. Purple represents identical residues; orange, similar residues. Percent identities and similarities of yeast Rvb1 or Rvb2 with human Rvb1 were generated by pairwise alignment using the EMBOSS water pairwise alignment algorithm on the European Bioinformatics Institute Web site [http://www.ebi.ac.uk/emboss/align/index.html]. Domains are boxed in their respective colors according to the X-ray crystal structure of human Rvb1.[24] Sequences that are part of the αβα subdomain of the AAA$^+$ domain are boxed in red, while those that are part of the putative DNA/RNA binding domain (the insertion domain) are boxed in light green. The C-terminal all-α subdomain of the AAA$^+$ domain is boxed in blue. Several consensus motifs are also highlighted based on the alignment of Neuwald *et al.*[27] and on the solved structure of human Rvb1.[24]

which are not well characterized. Here we show that Rvb1 alone and Rvb2 alone are active ATPases and helicases *in vitro*. We also show that yeast Rvb1 and Rvb2 form a heterohexameric single-ring complex that has enhanced ATPase and helicase activities compared with the individual components. We also demonstrate that the Rvb1/2 complex undergoes nucleotide-dependent conformational changes as observed by electron microscopy. These results reveal that the yeast Rvb proteins exhibit the hallmark features of AAA^+ helicases.

Results

The Rvb1 and Rvb2 proteins form a tight heterohexameric complex

The *RVB1* and *RVB2* genes were cloned from *Saccharomyces cerevisiae* genome and subsequently expressed in *Escherichia coli* and purified as described in Materials and Methods. Both proteins were judged to be more than 98% pure by SDS-PAGE analysis.

Size-exclusion chromatography analysis was first carried out in order to assess the oligomeric state of each protein alone (Fig. 2a). Considering that the theoretical molecular mass of Rvb1 is 50.5 kDa and that of Rvb2 is 51.6 kDa, both Rvb1 and Rvb2 alone eluted at the expected elution volume for a monomer (30–60 kDa) at 5 μM monomer concentration (Fig. 2a). However, both proteins formed higher-order oligomers (200–700 kDa) when higher concentrations were employed (40 μM). The addition of ADP (Fig. 2a) and that of ATP (not shown) did not significantly affect the observed elution profiles.

Rvb1 and Rvb2 were first preincubated at 4 °C for 4 h prior to injection on the size-exclusion chromatography column to analyze the oligomeric state of the Rvb1/2 complex. Unlike Rvb1 and Rvb2 alone,

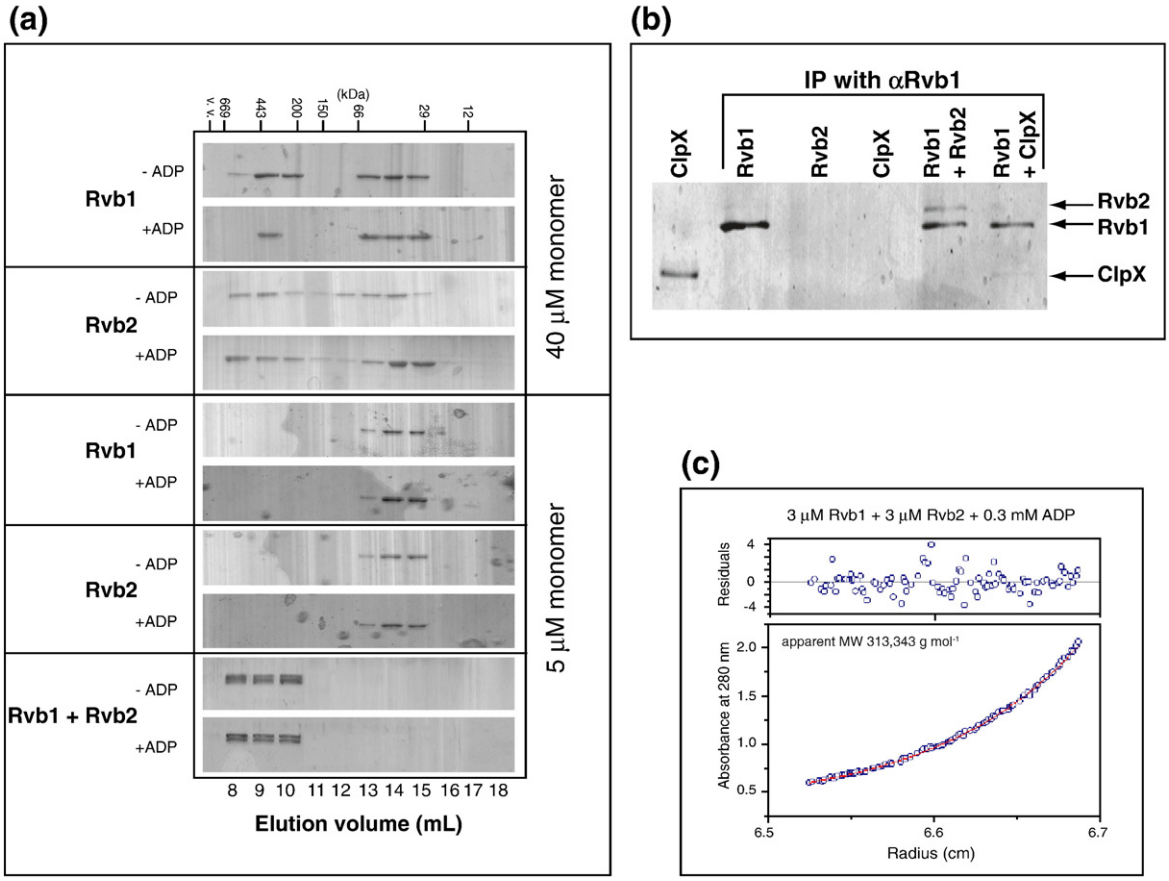

Fig. 2. Influence of protein concentration on the oligomerization of Rvb proteins. (a) Rvb1 and Rvb2 proteins as well as the Rvb1/2 complex were incubated at different concentrations for 4 h on ice in buffer B with or without addition of 1.5 mM ADP and then loaded on a Superdex 200 HR 10/30 column (Amersham Biosciences) equilibrated with the same buffer. Fractions were collected at 1-mL intervals, and proteins were then visualized on SDS-PAGE gels by silver staining. The positions of the molecular mass standards (in kilodaltons) are given along the upper *x*-axis. (b) Purified Rvb1, Rvb2, and ClpX (3 μM) were incubated for 4 h at 4 °C in buffer B. αRvb1 antibodies cross-linked to Protein A–Sepharose beads were added to the purified proteins and incubated for 1 h at 4 °C. The immunocaptured proteins were washed, eluted from the beads, separated on SDS-PAGE gel, and visualized with silver staining. (c) Lower panel shows the sedimentation equilibrium profile of a mixture of 3 μM Rvb1 + 3 μM Rvb2 in the presence of 0.3 mM ADP plotted as absorbance at 280 nm *versus* radius measured from the center of rotor. Solid line represents the best fit to the data. The corresponding distribution of the residuals is shown in the upper panel.

the Rvb1/2 complex eluted as a large oligomer even at low protein concentrations (Fig. 2a). The addition of ADP (Fig. 2a) and that of ATP (not shown) did not affect the elution profiles observed.

Affinity-purified αRvb1 antibodies were used to immunocapture Rvb1 from a mixture of 3 μM Rvb1 and 3 μM Rvb2 in order to explicitly demonstrate that the large oligomers observed when Rvb1 and Rvb2 proteins are mixed together (Fig. 2a) are a heterocomplex of Rvb1 and Rvb2. As shown in Fig. 2b, Rvb2 was coimmunocaptured with Rvb1, indicating that the complexes observed result from a direct interaction between the two proteins. The specificity of the antibodies used is demonstrated by the fact that the αRvb1 antibodies do not immunocapture Rvb2 alone or ClpX, an unrelated AAA^+ protein (Fig. 2b).

Sedimentation equilibrium analytical ultracentrifugation experiments were carried out on a mixture of 3 μM Rvb1 and 3 μM Rvb2 in the presence of 0.3 mM ADP to obtain a more accurate determination of the oligomeric state of the Rvb1/2 complex. Data were best fit to a single-species model with an apparent molecular mass of 313±15 kDa (Fig. 2c). This corresponds to a hexameric assembly of the Rvb1 and Rvb2 proteins.

The results shown in Fig. 2 clearly indicate that Rvb1 and Rvb2 tightly interact to form a heterohexameric complex.

The Rvb1/2 complex forms a 6-fold symmetrical single-ring particle

Transmission electron microscopy (TEM) studies combined with single-particle image processing were carried out in order to further analyze the structure of the Rvb helicases. The Rvbs were incubated at 2 μM concentration (1 μM Rvb1 + 1 μM Rvb2) with ADP, ATP, or ATPγS, and the samples were subsequently imaged at the electron microscope.

Abundant ring-shaped particles were observed when Rvb1 and Rvb2 proteins were mixed (Fig. 3a–c). They were consistently more abundant when both proteins were mixed in the presence of ADP (Fig. 3a) than in the presence of ATP (Fig. 3b) and that of ATPγS (Fig. 3c). Larger irregular particles were also observed, but they constituted only 5% of observed particles. Consistent with the chromatography experiments at low protein concentration (5 μM, Fig. 2a), ring-shaped particles were not observed in samples containing only one of the Rvb proteins.

Micrographs of the complex in the presence of ADP were digitized and analyzed using algorithms capable of detecting rotational symmetries in order to formally establish the symmetry of the ring-shaped Rvb1/2 particles.[29] Sixfold symmetry was detected mostly at a radius of 63.5 Å, which corresponds to the outer ring of the particle. The analysis was repeated with images of rings assembled in the presence of ATP and ATPγS, also detecting 6-fold symmetry. Results for the *t* test and the spectral ratio product are shown in Table 1. Interestingly, no other order of symmetry was found to be statistically significant.

Since only top views were observed for these particles and none of the images observed could be interpreted as side views, we could not determine from these micrographs whether Rvb1 and Rvb2 assemble into single-ring structures, double-ring structures, or higher-order ring structures. Thus, we used scanning TEM (STEM) to determine whether Rvb1/2 complexes form single-ring structures or higher-order ring structures. In images obtained by STEM, the intensity at any pixel is directly proportional to the mass, providing quantitative information of the particle mass. The absolute accuracy of this method for particles in the range of mass expected for the Rvb1/2 complexes is ~10%.[30] Therefore, although this method may not be sensitive enough to determine the number of subunits per ring, it is adequate to establish whether the Rvb1/2 complex has a single- or double-hexameric ring structure.

Samples containing the Rvb1 and Rvb2 proteins in the presence of nucleotide were freeze dried on carbon films, and STEM images were recorded. Round particles appeared in the images (Fig. 3d), and the mass of these particles was calculated as detailed in Materials and Methods. A few larger irregular particles were also observed by STEM, but, similarly to the TEM images, they only accounted for less than 5% of particles. The histograms of the round particles in Fig. 3e display a unimodal distribution of particles in the different nucleotide states centered at the mass expected for a single-hexameric ring. Significantly, no particle was found with the mass expected for a double-hexameric ring. The mean and SD of the data set obtained from the samples in the presence of ADP, ATP, and ATPγS are shown in Fig. 3e.

Hence, the data from the STEM and TEM experiments together with the results from the size-exclusion chromatography and sedimentation equilibrium experiments strongly suggest that the Rvb1 and Rvb2 proteins assemble predominantly into a single-hexameric ring structure.

Rvb1, Rvb2, and Rvb1/2 are active ATPases

Rvb proteins are members of the AAA^+ family and hence are expected to be active ATPases. Nevertheless, there has been some controversy about the ability of these proteins, derived from different organisms, to hydrolyze ATP. Here we investigated the ATPase activities of the yeast Rvb1 and Rvb2 proteins and whether DNA affects these activities.

Initially, we studied the dependence of the ATP hydrolysis rates on Rvb concentrations. Increasing concentrations of Rvb1, Rvb2, or preformed Rvb1/2 complex were incubated with ATP, and the initial hydrolysis rates were measured. As shown in Fig. 4a, Rvb1 and Rvb2 alone are active ATPases but the Rvb1/2 complex hydrolyzed ATP much

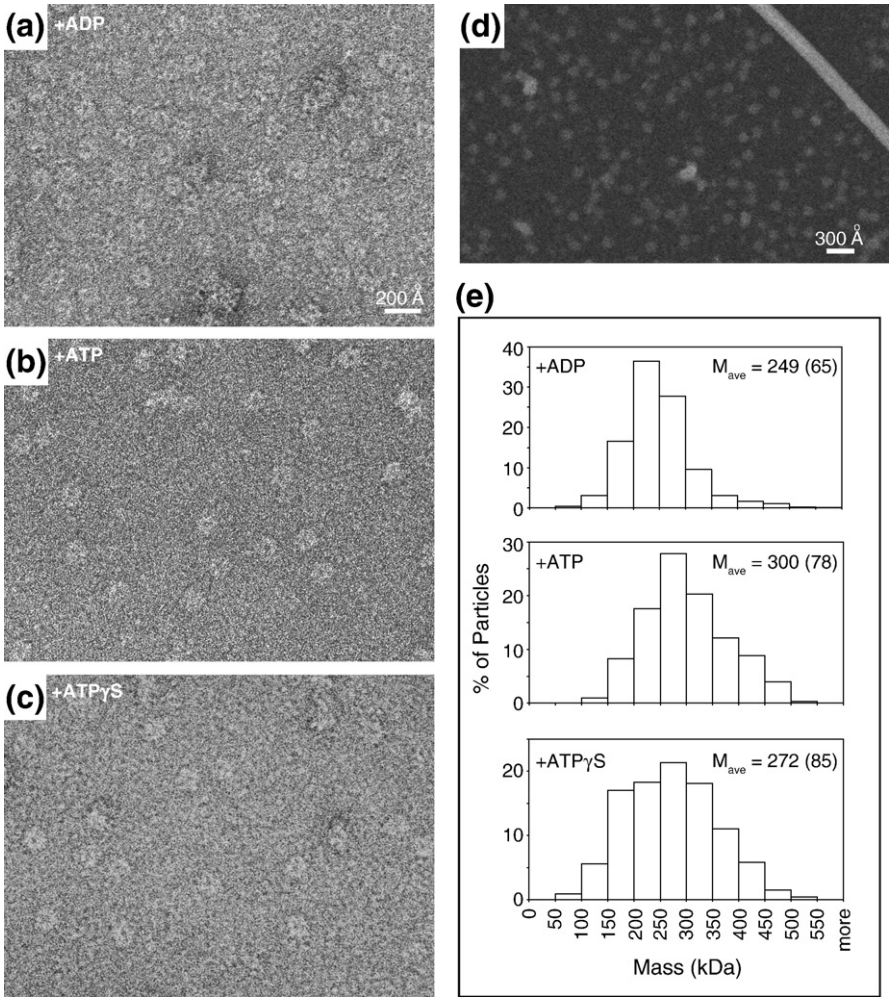

Fig. 3. The Rvb1/2 complex forms single rings as observed by electron microscopy. (a–c) TEM micrographs of negatively stained ring-shaped particles obtained upon incubation of Rvb1 and Rvb2 proteins with different nucleotides. (d) STEM micrographs of assembled ring-shaped Rvb1/2 complexes mixed with TMV rods. (e) The histograms were obtained from STEM micrographs and show the mass distribution of the particles in the presence of different nucleotides. The average mass (M_{ave}) and the SD (in parentheses) for each data set are shown.

more efficiently especially at monomer concentrations higher than 4 μM.

Complete Michaelis–Menten kinetic analysis was performed on Rvb1 (5 μM), Rvb2 (5 μM), and preformed Rvb1/2 complex (2.5 μM Rvb1 + 2.5 μM Rvb2). Rvb1/2 complex has higher k_{cat} and lower K_M than those of Rvb1 alone, which are better than those of Rvb2 alone (Fig. 4b).

We next investigated the effect of various DNA substrates on the ATPase activity of the Rvbs. As shown in Fig. 4c, circular double-stranded DNA (dsDNA, p11 circular, pETM60 circular), circular single-stranded DNA (ssDNA circular), linear dsDNA with blunt ends (p11 b_b), and total yeast RNA had no effect on the ATPase activity of the Rvbs. However, linear dsDNA containing at least one 5′ or 3′ overhang (p11 5′_5′, p11 3′_3′, pETM60 b_5′, *pih1* DNA b_5′) resulted in about twofold enhancement of the ATPase activity of the Rvb1/2 complex but not that of Rvb1 or Rvb2 alone.

Although we did not observe an effect of DNA on the initial ATP hydrolysis rates of Rvb1 and Rvb2 alone, the presence of linearized dsDNA with one protruding 5′ end (pETM60 b_5′) nevertheless allowed Rvb1 and Rvb2 as well as the Rvb1/2 complex to hydrolyze ATP for longer times (Fig. 4d). No such effect was observed using circular ssDNA (data not shown). Attenuation of ATP hydrolysis with time may be explained by an accumulation of ADP that would directly compete with ATP or that the generated ADP might cause a conformational change in the Rvbs resulting in reduced ATP hydrolysis efficiency. The DNA substrate may stabilize a certain Rvb protein conformation that prevents

Table 1. Analysis of the rotational symmetry of the Rvb1/2 ring-shaped particles

Nucleotide	Particles analyzed	Symmetry detected	*t* test and significance level (*p*)	Spectral ratio product
ADP	915	6	<0.000001	1.08×10^{17}
ATP	1271	6	<0.000001	5.11×10^{34}
ATPγS	1041	6	<0.000001	1.31×10^{81}

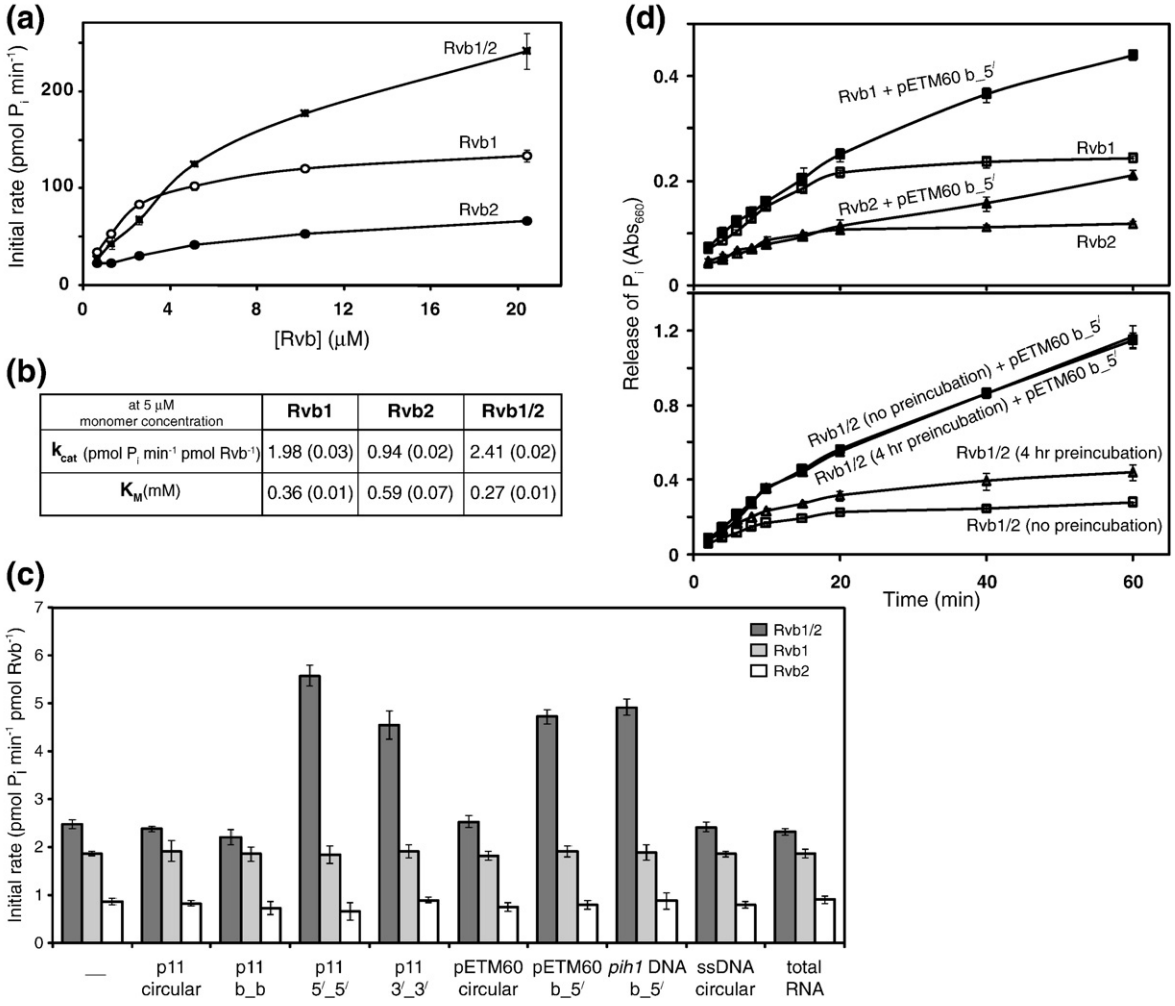

at 5 μM monomer concentration	Rvb1	Rvb2	Rvb1/2
k_{cat} (pmol P_i min^{-1} pmol Rvb^{-1})	1.98 (0.03)	0.94 (0.02)	2.41 (0.02)
K_M(mM)	0.36 (0.01)	0.59 (0.07)	0.27 (0.01)

Fig. 4. Rvb proteins are active ATPases. (a) Dependence of ATP hydrolysis rates on the concentration of the Rvb proteins. Shown are the initial rates for ATP hydrolysis at different concentrations of Rvb proteins in the presence of 4 mM ATP. The curves become linear above ~4 μM Rvb monomer concentration. For the Rvb1/2 complex, Rvb1 and Rvb2 proteins were preincubated for 4 h at 4 °C prior to addition of ATP. (b) k_{cat} and K_M were calculated for the Rvb proteins at 5 μM Rvb1 and 5 μM Rvb2 and for a preformed complex of 2.5 μM Rvb1+2.5 μM Rvb2 (monomer concentrations). (c) Enhancement of ATP hydrolysis rates of the Rvb proteins by linear DNA substrate. Different DNA or RNA substrates were added to 5 μM Rvb1, 5 μM Rvb2, and a preformed complex of 2.5 μM Rvb1+2.5 μM Rvb2 (monomer concentrations). Initial rates of ATP hydrolysis were measured in the presence of 5 pmol of DNA or RNA substrates. See Materials and Methods for the description of the substrates used. (d) Hydrolysis of ATP by 5 μM Rvb proteins was monitored as a function of time in the absence or presence of 5 pmol of linear DNA (pETM60 b_5′) (upper panel). The Rvb proteins and linear DNA were preincubated at room temperature for 10 min prior to addition of ATP. For the Rvb1/2 complex (lower panel), either linear DNA was directly mixed with 2.5 μM Rvb1 and 2.5 μM Rvb2 or the Rvb proteins were first preincubated for 4 h at 4 °C prior to addition of linear DNA and then ATP. The release of P_i was measured by the colorimetric assay at 660 nm as described in Materials and Methods.

inhibition by ADP, which seems to indicate that the Rvbs, alone or in complex, are functionally more efficient in the presence of DNA. The results shown in Fig. 4d indicate that Rvb1 and Rvb2 alone bind DNA, although DNA does not significantly enhance their initial ATP hydrolysis rate.

Observation of the nucleotide-dependent conformational changes in the Rvb1/2 complex by electron microscopy

Based on the above results, we speculated that the Rvbs might undergo nucleotide-dependent conformational changes, as has been described for other members of the AAA^+ superfamily. To this end, we obtained the two-dimensional averages of the Rvb1/2 complex in the presence of ADP, ATP, and ATPγS. In these experiments, Mg^{2+} was not added to the buffers to reduce ATP and ATPγS hydrolyses (see Materials and Methods).

Nearly all the particles observed in the electron micrographs were oriented with the 6-fold symmetry axis perpendicular to the grid. Thus, particle images were selected from micrographs and aligned by correlation averaging to calculate an average of the top views for each nucleotide state. The two-

dimensional average of the ring-shaped particles in the presence of ADP showed a hexagon with straight edges measuring ~142 Å between opposite vertices and with a heavily stained area of ~17 Å in diameter at the center of the particle that may represent a channel (Fig. 5, columns 1 and 2, ADP). Interestingly, the projection structure of the ring-shaped particles in the presence of ATP (Fig. 5, columns 1 and 2, ATP) showed dramatic structural differences compared with the ADP structure. In the presence of ATP, Rvb1/2 complex also showed a slightly bigger hexagon that measured ~152 Å between opposite vertices and had a smaller (~15 Å in diameter) stain-penetrated area at the center of the particle. The ATP hexagon had concave edges and some radial areas of stain penetration instead of the smooth stain-excluded area observed in the ADP form. As expected, the obtained two-dimensional average in the presence of ATPγS was very similar to and had dimensions identical with the one obtained for the ATP state (Fig. 5, columns 1 and 2, ATPγS).

Next, we evaluated the heterogeneity of the Rvb1/2 complexes assembled in the presence of ADP, ATP, and ATPγS. To do this, we carried out a reference-free two-dimensional image classification of the particles extracted from the electron micrographs. Resulting class averages from this classification method should show all variations present in the data regardless of source. Because in this data set all the particles represent the same orientation, with the 6-fold symmetry axis perpendicular to the grid, the variation shown in the class averages is due to multiple conformations. The two-dimensional class averages obtained in the presence of ADP produced four class averages resembling the ADP state with minor differences between them, which were interpreted as resulting from minor structural differences induced by the stain (Fig. 5, columns 3–6, ADP).

An identical classification approach for the rings assembled in the presence of ATP showed that about 9% of the selected particles are in fact in the ADP conformation (Fig. 5, column 3, ATP), which could be the result of some ATP hydrolysis by the helicases in the absence of added Mg^{2+}. The other three class averages obtained from this sample resembled the ATP state (Fig. 5, columns 4–6, ATP), and the classification approach separated particles that had clockwise features (Fig. 5, columns 5 and 6, ATP) from those that had counterclockwise features (Fig. 5, column 4, ATP). These two classes of particles represent top and bottom views of the structure. Particles that had clockwise features were split into two classes (Fig. 5, columns 5 and 6, ATP) by the classification program probably because small differences in the stain accumulated at the edge of the particles.

For the sample in the presence of ATPγS, all four class averages obtained resembled the ATP state (Fig. 5, columns 3–6, ATPγS). Similarly, the classification approach separated particles that had clockwise features (Fig. 5, column 4, ATPγS) from those that had counterclockwise features (Fig. 5, columns 5 and 6, ATPγS). A fourth group of particles that showed no specific orientation of features was found. This group represents particles that were distorted or flattened during the staining process.

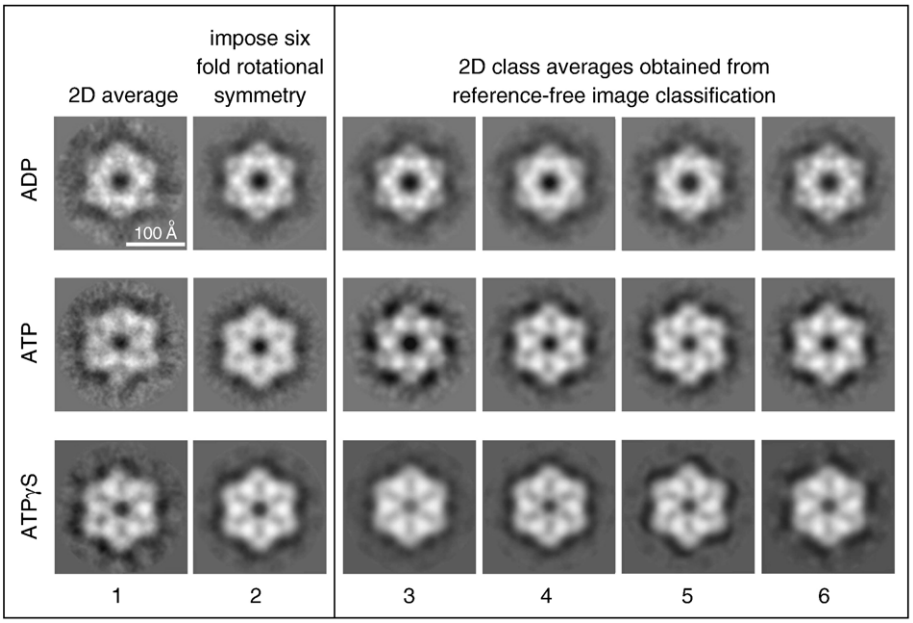

Fig. 5. Structures of the hexameric ring-shaped Rvb1/2 complexes depend on the nature of the bound nucleotide. Shown are projection structures of the ring-shaped Rvb1/2 particles in the presence of different nucleotides. Images shown in the different columns are as follows: (1) two-dimensional averages of the ring-shaped particles; (2) two-dimensional averages obtained by imposing 6-fold rotational symmetry to the averages in (1); and (3–6) resulting class averages obtained from a reference-free image classification analysis of the full set of ring-shaped particle images.

These results confirm that the Rvb1/2 complex exhibits a nucleotide-dependent conformational change.

Rvb1, Rvb2, and Rvb1/2 are active helicases

The above results clearly demonstrate the ability of the Rvb proteins to interact with DNA, to hydrolyze ATP, and to undergo nucleotide-dependent conformational changes. Consequently, experiments were carried out to determine if the Rvbs function as active helicases. A radiolabeled 15-nucleotide-long DNA primer was annealed onto single-stranded M13mp18 plasmid and incubated with the Rvbs in the presence or absence of ATP. As shown in Fig. 6a, Rvb1, Rvb2, and Rvb1/2 were all able to release (unwind) the bound oligonucleotide in an ATP-dependent manner. However, Rvb1 and Rvb2 alone have weak helicase activity, with similar rates of unwinding (data not shown). In addition, Rvb2 is able to unwind a greater amount of substrate compared with Rvb1. The Rvb1/2 complex exhibits greater helicase activity both in rate of unwinding and in amount of oligonucleotide released compared with Rvb1 and Rvb2 alone, with complete unwinding of substrate observed at 45 min. Quantitative analysis of the data from several experimental replicates indicates that the Rvb1/2 complex unwinds about two to three times faster than Rvb1 and Rvb2 alone, demonstrating that Rvb1 and Rvb2 in complex act synergistically to unwind DNA duplexes.

The preferential directionality of the helicase activity of the Rvbs was assessed using a substrate consisting of a 28-nucleotide-long primer annealed onto a 43mer, for 3′-to-5′ directionality test, or a 45mer, for 5′-to-3′ directionality test (Fig. 6b). Directionality is given with respect to the ssDNA flanking the duplex. Rvb1 and Rvb2 alone exhibited no significant helicase activity on either substrate, but the Rvb1/2 complex was able to unwind the 28-nucleotide-long primer, with strong preference for unwinding in the 5′-to-3′ direction (Fig. 6b). With the use of shorter primers, the data suggest that Rvb1 and Rvb2 alone have weak preferential 5′-to-3′ unwinding activities as well (not shown).

It is important to note that although Rvb1 and Rvb2 alone are capable of releasing a 15-nucleotide-long primer (Fig. 6a), they were not able to release a 28-nucleotide-long primer (Fig. 6b). Furthermore, Rvb2 was unable to release a 40-nucleotide-long primer from M13mp18 (data not shown). These results suggest that each component alone has limited processivity and that the Rvb1/2 complex is probably the physiologically efficient helicase.

The above experiments clearly establish the Rvbs as active helicases whether alone or in complex.

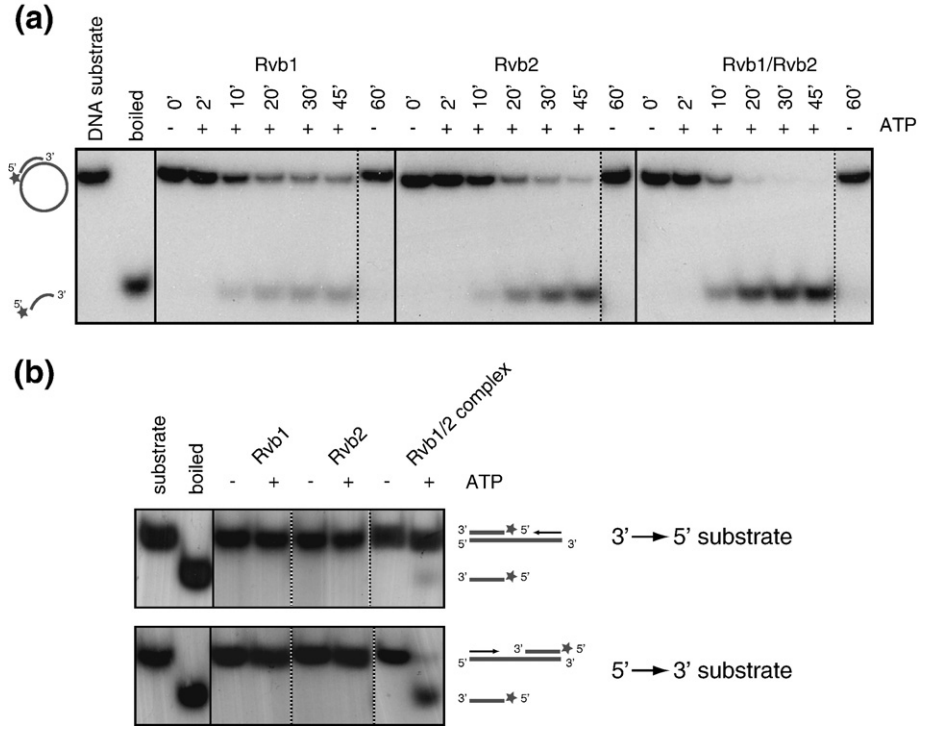

Fig. 6. Rvb proteins are active helicases. (a) Helicase activity assays of the Rvb proteins. Rvb1 and Rvb2 proteins as well as the Rvb1/2 complex were incubated with the indicated DNA substrate consisting of an oligonucleotide labeled at the 5′ end annealed to M13 ssDNA circular plasmid. The reaction was initiated by the addition of ATP. At different time points, aliquots were removed and the bound and released radiolabeled oligonucleotides were visualized on 10% native TAE-PAGE gels. Schematics are shown on the left. Stars indicate the position where the oligonucleotide was labeled with ^{32}P. (b) The preferential directionality of the Rvb helicase activities was assessed using 5′-to-3′ and 3′-to-5′ substrates, shown in cartoon representation on the right, next to their gel positions. Arrows indicate the proposed direction of translocation of the helicase.

However, the Rvb1/2 complex seems to be the most competent helicase.

Discussion

The ATPase and helicase activities of the Rvbs

In this study, we have clearly established that yeast Rvb1 and Rvb2 proteins, whether alone or in complex, are active ATPases and helicases. The nature of the activities of the Rvb proteins has been rather controversial since several published studies have yielded conflicting results. The different conclusions reached by various groups could be attributed to the different methods used to purify the proteins, could be the result of buffer conditions employed in the assays, or might be true differences between Rvbs from different species.

One group found that rat Rvb1[28] and human Rvb2[3] have an ATPase activity that was stimulated by ssDNA but not dsDNA. In that particular study, rat Rvb1 was found to have 3′-to-5′ helicase activity, while human Rvb2 exhibited 5′-to-3′ activity.[3] In contrast to these results, two groups found that human Rvb1 had no or marginal ATPase activity and no helicase activity.[2,24] However, more recently, Puri *et al.*[16] found that human Rvb1 and Rvb2 are active as ATPases but that DNA did not stimulate their activity.

Our results clearly demonstrate that the yeast Rvb1 and Rvb2 proteins and the Rvb1/2 complex are active ATPases, with the Rvb1/2 complex having the highest activity, followed by Rvb1 and then by Rvb2 (Fig. 4a). Hence, the ATPase activity of the individual Rvb proteins is significantly improved by the formation of the Rvb1/2 complex as indicated by the k_{cat} and K_M values (Fig. 4b). These values are comparable with those measured for *E. coli* RuvB[31] and with those published by Ikura *et al.*[22] for the yeast Rvbs.

Our data also show that the Rvb proteins are ATP-dependent helicases since the presence of ATP was required for helicase activity (Fig. 6). Furthermore, we found that specific DNA substrates stimulated the ATPase activity. As shown in Fig. 4c, the ATPase activity of the Rvb1/2 complex is dramatically enhanced in the presence of linear dsDNA with 5′ or 3′ overhangs. In addition, we observed that although the presence of DNA did not change the initial ATP hydrolysis rates obtained for Rvb1 and Rvb2 alone, it allowed Rvb1 and Rvb2 as well as the Rvb1/2 complex to hydrolyze ATP for longer times. These data indicate an interdependency of the helicase and ATPase activities.

Based on our helicase assays, we observed that Rvb1/2 unwinds DNA more efficiently compared with Rvb1 and Rvb2 alone. In addition, Rvb2 seems to be able to unwind a greater amount of substrate compared with Rvb1 (Fig. 6a), although Rvb2 has a lower ATPase activity compared with Rvb1 in the presence or absence of DNA (Fig. 4). The 5′-to-3′ preferential directionality of the Rvb1/2 helicase (Fig. 6b) is similar to that reported for human Rvb2[3] and for *E. coli* RuvAB[32] but opposite of the polarity observed for rat Rvb1.[28]

The mechanism by which the Rvb1/2 complex binds and unwinds DNA substrate remains to be elucidated. It has been suggested that the insertion domain in the Rvbs (Fig. 1) is a novel DNA/RNA binding domain.[24] The Rvb1/2 hexamer most likely opens up to allow single-stranded nucleic acid to bind the central channel. This is supported by the fact that the Rvb1/2 complex is able to release a 15mer nucleotide from single-stranded circular M13 plasmid (Fig. 6a). This is also supported by our electron microscopy analyses in which the central channel of the Rvb1/2 hexameric complex is ~15–17 Å in diameter (Fig. 5), large enough to accommodate ssDNA, but not dsDNA. The diameter of the central channel is comparable with that of other helicases, such as the E1 helicase from Papillomavirus,[33] in which the crystal structure shows a central channel diameter of 20 Å occupied by ssDNA. It has been proposed that ring-shaped helicases can bind one DNA/RNA strand through their central channel, while the other strand contacts the outside of the ring. This has been shown for the bacteriophage T7 gp4D helicase[34,35] and for the Rho helicase.[36,37] Such a mechanism might also apply for the Rvb1/2 hexamer.

The oligomeric state of the Rvb1/2 complex

Helicases can function as monomers, dimers, or larger oligomers. Importantly, a large number of helicases oligomerize into homohexameric rings, including viral (T7 gp4 and T4 gp41), bacterial (DnaB and RuvB), and eukaryotic (human Bloom's syndrome helicase) helicases.[38] Size-exclusion chromatography indicated that Rvb1 and Rvb2 exist mainly as monomers at low concentrations but form larger oligomers in a concentration-dependent manner (Fig. 2a). Equilibrium sedimentation analysis performed on a range of concentrations for Rvb1 and Rvb2 also indicated the heterogeneity of these samples (data not shown). These results agree with the observation that human Rvb1 forms hexamers under the high concentration conditions used for X-ray crystallography[24] and with the observation of multiple oligomeric states for human Rvb2.[16] Also, monomers of the bacterial RuvB have been shown to cooperatively assemble into higher oligomers in a concentration-dependent manner.[39]

Incubation of Rvb1 and Rvb2 proteins resulted in the formation of a large complex that was shown to correspond to a hexamer by equilibrium sedimentation experiments (Fig. 2c) and electron microscopy (Figs. 3 and 5 and Table 1). The immunocapture experiment illustrated in Fig. 2b and the observation by electron microscopy of antibody-labeled hexameric rings using affinity-purified αRvb1 and αRvb2 antibodies (data not shown) demonstrate the presence of both Rvb1 and Rvb2 proteins in the hexameric rings. Size-exclusion chromatography

experiments as illustrated in Fig. 2a and our prior *in vivo* pull-down experiments[15] suggest the presence of equimolar concentrations of Rvb1 and Rvb2 in the Rvb1/2 complex.

Our finding that yeast Rvb1 and Rvb2 form a single-hexameric ring is in contrast with the finding that human Rvb1 and Rvb2 form a double-hexameric ring.[16] This is rather surprising since human and yeast Rvbs share ~70% sequence identity (Fig. 1). The difference either could be due to the purification protocols used, especially since the human Rvbs purified by Puri *et al.*[16] were inactive as helicases, which contradicts the findings of Kanemaki *et al.*,[3] or might be an actual difference between the human and yeast Rvbs. In support of the latter possibility, it was found that the deletion of the two yeast *RVB* genes cannot be complemented by human, mouse, and rat Rvbs,[2,11] indicating a possible structural difference between yeast and mammalian Rvbs.

The oligomeric state of the Rvb proteins when acting as helicases needs to be further considered. Our data showed that the highest helicase activity was observed when Rvb1 and Rvb2 together were incubated with ATP. This condition correlates with the presence of heterohexameric rings in the electron micrographs. The same correlation exists with respect to the ATPase activity. These results strongly support the conclusion that the functional form of these proteins is the heterohexameric ring. Interestingly, a ring-like arrangement is not uncommon in proteins involved in DNA metabolism because this is proposed to increase the processivity of the enzymes.[40] However, we also observed lower helicase and ATPase activities when only Rvb1 or Rvb2 was present in the reaction, under conditions in which we were not able to observe ring-shaped particles for these proteins. Hence, it is possible that each protein alone can act as a helicase as some other lower-order oligomer, as has been reported for RecQ[41] and UvrD.[42]

In conclusion, our study has demonstrated that the yeast Rvbs are active ATPases and are ATP-dependent helicases that form heterohexameric ring structures that undergo nucleotide-dependent conformational changes. These findings show that the yeast Rvb proteins fulfill the main defining features of the AAA^+ superfamily of proteins. Our work sets the stage for future investigations to unveil the structural details of the mechanism of function of this essential family of helicases.

Materials and Methods

Recombinant protein expression, purification, and manipulation

The Rvb1 and Rvb2 genes were PCR amplified from yeast *S. cerevisiae* S288C genomic DNA and cloned into pProEX HTb expression vector (Invitrogen) for the Rvb1 protein and into p11 expression vector for the Rvb2 protein.[43] Both proteins were expressed as N-terminal His_6–tobacco etch virus protease fusion proteins in *E. coli* BL21(DE3) gold (pRIL) and purified using Ni–nitrilotriacetic acid resin (Qiagen) according to the manufacturer's protocols. The purified proteins were dialyzed and stored in buffer A (25 mM Tris–HCl, pH 7.5, 200 mM KCl, 1 mM DTT, and 10% glycerol). Tobacco etch virus protease was used to remove the His_6 tag to generate untagged proteins. The proteins were further purified on a Bio-Scale CHT5-I hydroxyapatite column (BioRad) and a MonoQ column (Amersham Biosciences). The concentrations of purified Rvb1 and Rvb2 were determined using the Bradford assay method.[44] All molar concentrations are typically given for monomers except as indicated.

Size-exclusion chromatography

Size-exclusion chromatography was performed using a calibrated Superdex 200 HR 10/30 column (Amersham Biosciences) attached to an AKTA FPLC system (Amersham Biosciences). The column was equilibrated with buffer B (25 mM Tris–HCl, pH 7.5, 200 mM KCl, 5 mM $MgCl_2$, 1 mM DTT, and 10% glycerol). The molecular mass standards (Sigma) used were as follows: thyroglobulin, 669 kDa; apoferritin, 443 kDa; β-amylase, 200 kDa; alcohol dehydrogenase, 150 kDa; bovine serum albumin, 66 kDa; carbonic anhydrase, 21 kDa; and cytochrome *C*, 12.4 kDa. All experiments were performed at 4 °C, and absorbance was monitored at 280 nm. Nucleotides were added to the buffer as needed. For the Rvb1/2 complex, an equal amount of Rvb1 and Rvb2 proteins was preincubated for 4 h at 4 °C to ensure proper complex formation prior to use in assays.

Sedimentation equilibrium analysis of Rvb proteins

Sedimentation equilibrium experiments and analysis were performed at the Ultracentrifugation Service Facility at the University of Toronto Department of Biochemistry. Rvb1 and Rvb2 proteins as well as the preformed Rvb1/2 complex were at a 6 μM monomer concentration in buffer B, and 0.3 mM ADP was added. Samples were spun at 6000, 8000, 10,000, and 14,000 rpm at 4 °C in a Beckman Optima XL-A analytical ultracentrifuge using an An-60 Ti rotor. Absorbance was monitored at 230 and 280 nm. Data analysis was performed using the Origin MicroCal XL-A/CL-I Data Analysis Software Package version 4.0.

Measurement of the ATPase activity of the Rvb proteins

The ATPase activity of the Rvb proteins was measured by determining the free phosphate released after ATP hydrolysis using a colorimetric assay as described previously.[45] Briefly, Rvb proteins were placed in buffer B, containing various concentrations of ATP. However, buffer C (25 mM Tris–HCl, pH 7.5, 25 mM KCl, 5 mM $MgCl_2$, 1 mM DTT, and 10% glycerol) was used when DNA or RNA substrates were added. Assays were performed in 200-μL volumes at 37 °C in a quartz plate. At different time points, 10-μL aliquots of the assay mixture were removed and added to 200 μL of color developing solution (1 mM malachite green, 8.5 mM ammonium molybdate, and 1 M HCl). Color development was allowed to proceed for 1 min and was then stopped by the addition of 25 μL of 37% citric acid. Absorbance was measured at 660 nm and converted to moles of phosphate produced using a KH_2PO_4 standard curve.

Initial rates were derived from data collected in the first 10 min of the reactions.

The DNA/RNA substrates used in the assays were as follows:

p11 circular (5708 bp): from Ref. 43;
p11 b_b (680 bp; 1198 bp; 2263 bp; 1567 bp): p11 plasmid digested with RsaI in the presence of SAP to generate blunt ends;
p11 5′_5′ (5708 bp): p11 plasmid digested with EcoRI in the presence of SAP to generate 5′ protruding ends;
p11 3′_3′ (5708 bp): p11 plasmid digested with PstI in the presence of SAP to generate 3′ protruding ends;
pETM60 circular (7922 bp): from Ref. 46;
pETM60 b_5′ (6882 bp): pETM60, in which the *PIH1* gene was cloned and cut with NcoI, and then the linearized vector was mixed with T4 polymerase to fill the 5′ protruding ends; subsequently, the resulting DNA was digested with BamHI enzyme, which releases *PIH1*, to generate a linear DNA with one blunt end and one 5′ protruding end;
pih1 DNA b_5′ (1032 bp): corresponds to the released *PIH1* above;
ssDNA circular (7249 bases): single-stranded M13 DNA (M13mp18) was a generous gift from Dr. Igor Chevelev (University of Toronto);
total RNA: total yeast RNA was extracted with phenol chloroform and precipitated in 1/10 volume of 5 M LiCl and 2.5 volumes of ethanol.

Digested DNA was purified using an Invitrogen PCR purification kit.

Antibodies

Rabbit αRvb1 antibody was raised using Rvb1 protein expressed and purified from *E. coli*. The antibody was generated at the University of Toronto Division of Comparative Medicine and affinity purified on CNBr Sepharose beads to which purified proteins were cross-linked using established protocols.

Helicase assays

The preparation of DNA substrates was carried out as follows: For the experiment illustrated in Fig. 6a, 2 pmol of a 15mer DNA primer (GGA TCC CCG GGT ACC) was labeled at the 5′ end with 20 μCi of 6000 Ci/mmol [γ^{32}P] ATP (Perkin-Elmer) using T4 polynucleotide kinase (NEB) for 30 min at 37 °C and then stopped with 10 mM ethylenediaminetetraacetic acid (EDTA). An equimolar amount of single-stranded M13mp18 DNA was added to the mixture in hybridization buffer D (20 mM Tris–HCl, pH 7.5, 100 mM NaCl, 10 mM $MgCl_2$, and 1 mM DTT) and boiled for 5 min at 95 °C. The mixture was slowly cooled to room temperature to allow the primer to anneal to M13mp18. The mixture was applied to 1 mL of Sephadex G75 (Pharmacia) column, equilibrated with hybridization buffer, and the radioactivity in the collected fractions was quantified by liquid scintillation counting.

Four picomoles of a 28mer oligonucleotide (GAC TCT AGA GGA TCC CCG GGT ACC GAG C) was radiolabeled at the 5′ end with 40 μCi of 6000 Ci/mmol [γ^{32}P]ATP with T4 polynucleotide kinase to make the directionality substrates for the experiment illustrated in Fig. 6b. The reaction was stopped with 10 mM EDTA and incubated at 65 °C for 20 min. The mixture was then divided into two. One half was mixed with an equimolar amount of 43mer oligonucleotide A (GCT CGG TAC CCG GGG ATC CTC TAG AGT CAT TGC AGT GCA AGA C), and the other half was mixed with an equimolar amount of 45mer oligonucleotide B (ACA CTT ACG TGA CCT AAG CTC GGT ACC CGG GGA TCC TCT AGA GTC). Samples were boiled for 5 min at 95 °C and then slowly cooled to room temperature. Each mixture was applied to 1 mL of Sephadex G75 column, and purity was assessed by running the collected fractions on 10% TAE (Tris–acetate–EDTA)-PAGE gels. 28mer annealed to oligonucleotide A is the 3′-to-5′ substrate, while 28mer annealed to oligonucleotide B is the 5′-to-3′ substrate.

Helicase assay was carried out in a 10-μL reaction volume at 30 °C for 1 h. pH levels were varied, as well as the concentrations of protein, KCl, NaCl, $MgCl_2$, and ATP, to obtain optimal assay conditions. Both Rvb1 and Rvb2 performed optimally in buffer E (40 mM Tris–HCl, pH 7.5, 50 mM NaCl, 3 mM $MgCl_2$, and 10% glycerol) at a protein monomer concentration of 2.8 pmol/μL. ATP (1 mM) was added to start the reaction. The final concentration of 15mer DNA substrate, the 3′-to-5′ directionality substrate, and 5′-to-3′ directionality substrate was 16 μCi/μL (2.8 pmol/μL). For time course experiments, an 80-μL reaction volume was used and 10-μL samples were taken at time 0 before the addition of ATP and at 2, 10, 20, 30, and 45 min after the addition of ATP. Reactions were stopped with buffer F (50% glycerol, 50 mM EDTA, 0.6% SDS, 0.15% Bromophenol blue, and 0.19% xylene cyanol). All samples were run on 10% native TAE-PAGE gels. Radiolabeled oligonucleotide was detected by autoradiography.

TEM

Rvb1 and Rvb2 proteins were mixed in equimolar amounts to produce ring-shaped particles. Typically, Rvb1 and Rvb2 were combined in buffer A, and then ADP, ATP, or ATPγS was added to a final concentration of 1.5 mM. The final concentration of each protein during the assembly was 15 μM, and the volume of the assembly reaction was 20 μL. Assembly reactions with only one of the Rvb proteins present were performed in a similar manner. Proteins were usually incubated at 37 °C for 30 min, and then a 1/15 dilution of the mixture was applied to the electron microscopy grid. Incubations of 4 h at 4 °C were also used with similar results.

All samples were applied by floating a 10-μL drop to carbon-coated grids previously glow discharged and negatively stained with 2% uranyl acetate. Specimens were observed in a JEOL 2010F electron microscope operated at 200 kV. Images were collected at 50,000× with a dose of ~10 electrons/Å^2. All images were recorded on Kodak SO-163 films, scanned on a Nikon Super COOLSCAN 9000 ED at 6.35 μm/pixel, and averaged two times to produce data at 2.54 Å/pixel.

Single-particle image processing

Particles were extracted interactively from digitized fields using the Boxer (EMAN) program.[47] Normalized particles were translationally aligned relative to a previously obtained circularly symmetrical reference image produced by averaging the data set to perform the symmetry analysis. The presence of statistically significant rotational symmetry in the data was then assessed using two statistical tests, the spectral ratio product and Student's *t* test, as previously described.[29]

Cross-correlation methods were used in the classalign2 program (EMAN)[47] to align the ring-shaped particles and to obtain the two-dimensional averages. Typically, one particle of the data set was selected as a reference for the first cycle of alignment, averaging the aligned particles and then generating a second reference that was used in a subsequent alignment cycle. The process was iterated up to eight times to obtain the final two-dimensional average. The same procedure was followed starting with three particles as the initial reference to assess the robustness of the results and to prove non-model bias of the final two-dimensional averages.

The particle heterogeneity in the raw images was analyzed using a reference-free two-dimensional image classification implemented in the *refine2d.py* program in EMAN.[48] This method is equivalent to the multivariate statistical analysis that has been used classically in the single-particle processing field,[49] but in this case, the Eigen images are calculated from class averages initially obtained using rotational and radial harmonics of the power spectrum of the particles instead of the raw particles. The process was typically iterated eight times, and the class averages obtained at the end of each iteration were used to produce the Eigen images that seeded the multivariate statistical analysis of the next iteration.

STEM

Specimens were prepared according to the standard method of the Brookhaven National Laboratory STEM facility‡. Briefly, a 2-μL drop of a 100-μg/mL solution of tobacco mosaic virus (TMV), used as a calibration standard, was absorbed for 1 min onto freshly prepared carbon films supported on a holey membrane on a titanium grid. The grid was washed four times in water, and a 3-μL drop of a 1/10 dilution of previously assembled ring-shaped particles was applied to the grid for 1 min and thoroughly washed five times with 100 mM ammonium acetate and five more times with 20 mM ammonium acetate. The excess liquid was blotted with filter paper, and the grid was plunged into liquid nitrogen slush for quick freezing. The ~1-μm-thick ice layer was freeze dried by transferring the grid into an ion-pumped chamber and gradually increasing the temperature (overnight) to −80 °C. Grids were then transferred under vacuum to the STEM.

Images were collected on the Brookhaven National Laboratory 40-kV STEM with a 0.25-nm probe. Low-dose techniques were used to collect the images with an average electron dose <1000 e^-/nm^2, and the grid was kept at −150 °C during data collection, which keeps the mass loss <2% due to radiation damage. Images were collected digitally from the large detector (40–200-mrad acceptance angles) and used for mass determination. Large-angle signals are proportional to the mass in the irradiated pixel for thin specimens. Obtained images had a scan width of 0.512 μm.

Processing of STEM images

Mass measurements were made with the program PCMass29.[50] Particles were selected with a circular cursor, and the number of electrons scattered by the particle area was added and then subtracted from the number of electrons scattered from the background. The result was then multiplied by a standard calibration constant (115 Da/e^-) to determine the mass. The calibration constant was calculated using the TMV included in the specimen. Absolute scaling of the images was also done by using the TMV. First, in each image, as many measurements as possible were collected from the TMV particles and mass per length (M/L) average was calculated. Images with an SD in the M/L average greater than ±1.4 kDa/Å were rejected. Images with an average M/L for TMV of 13.1±1.4 kDa/Å were used directly for mass determination. Finally, for images with a TMV M/L average different from 13.1 kDa/Å, a scaling factor was calculated to bring the TMV M/L average to 13.1 kDa/Å. This scaling factor was then applied to the Rvb1+Rvb2 particles in these images. TMV M/L average was found to be very close to the expected 13.1 kDa/Å for most of the images. Histograms and statistics were obtained with Microsoft Excel.

‡ http://www.biology.bnl.gov/stem/specimen.html

Acknowledgements

This work was supported in part by grants from the National Cancer Institute of Canada (W.A.H.) and the National Science and Engineering Research Council of Canada (J.O.). We thank Dr. Igor Chevelev for his help with the helicase assays. We also thank Yulia Tsitrin, Reagan Ching, Keith Wong, Dr. Rongmin Zhao, and Dr. Yoshito Kakihara for contributing to different aspects of the project. Technical assistance from Fred Pearson and Andy Duft of the Canadian Centre for Electron Microscopy is acknowledged. In addition, we thank Drs. Martha Simon and Joseph Wall of the Brookhaven National Laboratory STEM for providing the STEM images. The Brookhaven National Laboratory STEM is a National Institutes of Health-Supported Resource Center (NIH 5 P41 EB2181), with additional support provided by the Department of Energy and the Office of Biological and Environmental Research. A.G. is a postdoctoral fellow of the Canadian Institutes of Health Research Training Program Grant in Protein Folding: Principles and Diseases. W.A.H. and J.O. are Canadian Institutes of Health Research New Investigators.

References

1. Kurokawa, Y., Kanemaki, M., Makino, Y. & Tamura, T. A. (1999). A notable example of an evolutionary conserved gene: studies on a putative DNA helicase TIP49. *DNA Sequence*, **10**, 37–42.
2. Qiu, X. B., Lin, Y. L., Thome, K. C., Pian, P., Schlegel, B. P. & Weremowicz, S. (1998). An eukaryotic RuvB-like protein (RUVBL1) essential for growth. *J. Biol. Chem.* **273**, 27786–27793.
3. Kanemaki, M., Kurokawa, Y., Matsu-ura, T., Makino, Y., Masani, A., Okazaki, K. *et al.* (1999). TIP49b, a new RuvB-like DNA helicase, is included in a complex together with another RuvB-like DNA helicase, TIP49a. *J. Biol. Chem.* **274**, 22437–22444.
4. Bauer, A., Chauvet, S., Huber, O., Usseglio, F., Rothbacher, U., Aragnol, D. *et al.* (2000). Pontin52 and

reptin52 function as antagonistic regulators of beta-catenin signalling activity. *EMBO J.* **19**, 6121–6130.
5. Shinagawa, H., Makino, K., Amemura, M., Kimura, S., Iwasaki, H. & Nakata, A. (1988). Structure and regulation of the *Escherichia coli* ruv operon involved in DNA repair and recombination. *J. Bacteriol.* **170**, 4322–4329.
6. West, S. C. & Connolly, B. (1992). Biological roles of the *Escherichia coli* RuvA, RuvB and RuvC proteins revealed. *Mol. Microbiol.* **6**, 2755–2759.
7. Kuzminov, A. (1993). RuvA, RuvB and RuvC proteins: cleaning-up after recombinational repairs in *E. coli*. *BioEssays*, **15**, 355–358.
8. Radovic, S., Rapisarda, V. A., Tosato, V. & Bruschi, C. V. (2007). Functional and comparative characterization of *Saccharomyces cerevisiae RVB1* and *RVB2* genes with bacterial Ruv homologues. *FEMS Yeast Res.* **7**, 527–539.
9. Jonsson, Z. O., Dhar, S. K., Narlikar, G. J., Auty, R., Wagle, N., Pellman, D. *et al.* (2001). Rvb1p and Rvb2p are essential components of a chromatin remodeling complex that regulates transcription of over 5% of yeast genes. *J. Biol. Chem.* **276**, 16279–16288.
10. Ohdate, H., Lim, C. R., Kokubo, T., Matsubara, K., Kimata, Y. & Kohno, K. (2003). Impairment of the DNA binding activity of the TATA-binding protein renders the transcriptional function of Rvb2p/Tih2p, the yeast RuvB-like protein, essential for cell growth. *J. Biol. Chem.* **278**, 14647–14656.
11. Lim, C. R., Kimata, Y., Ohdate, H., Kokubo, T., Kikuchi, N., Horigome, T. & Kohno, K. (2000). The *Saccharomyces cerevisiae* RuvB-like protein, Tih2p, is required for cell cycle progression and RNA polymerase II-directed transcription. *J. Biol. Chem.* **275**, 22409–22417.
12. Dugan, K. A., Wood, M. A. & Cole, M. D. (2002). TIP49, but not TRRAP, modulates c-Myc and E2F1 dependent apoptosis. *Oncogene*, **21**, 5835–5843.
13. King, T. H., Decatur, W. A., Bertrand, E., Maxwell, E. S. & Fournier, M. J. (2001). A well-connected and conserved nucleoplasmic helicase is required for production of box C/D and H/ACA snoRNAs and localization of snoRNP proteins. *Mol. Cell. Biol.* **21**, 7731–7746.
14. Watkins, N. J., Lemm, I., Ingelfinger, D., Schneider, C., Hossbach, M., Urlaub, H. & Luhrmann, R. (2004). Assembly and maturation of the U3 snoRNP in the nucleoplasm in a large dynamic multiprotein complex. *Mol. Cell*, **16**, 789–798.
15. Zhao, R., Davey, M., Hsu, Y. C., Kaplanek, P., Tong, A., Parsons, A. B. *et al.* (2005). Navigating the chaperone network: an integrative map of physical and genetic interactions mediated by the hsp90 chaperone. *Cell*, **120**, 715–727.
16. Puri, T., Wendler, P., Sigala, B., Saibil, H. & Tsaneva, I. R. (2007). Dodecameric structure and ATPase activity of the human TIP48/TIP49 complex. *J. Mol. Biol.* **366**, 179–192.
17. Shen, X., Mizuguchi, G., Hamiche, A. & Wu, C. (2000). A chromatin remodelling complex involved in transcription and DNA processing. *Nature*, **406**, 541–544.
18. Jin, J., Cai, Y., Yao, T., Gottschalk, A. J., Florens, L., Swanson, S. K. *et al.* (2005). A mammalian chromatin remodeling complex with similarities to the yeast INO80 complex. *J. Biol. Chem.* **280**, 41207–41212.
19. Krogan, N. J., Keogh, M. C., Datta, N., Sawa, C., Ryan, O. W., Ding, H. *et al.* (2003). A Snf2 family ATPase complex required for recruitment of the histone H2A variant Htz1. *Mol. Cell*, **12**, 1565–1576.
20. Mizuguchi, G., Shen, X., Landry, J., Wu, W. H., Sen, S. & Wu, C. (2004). ATP-driven exchange of histone H2AZ variant catalyzed by SWR1 chromatin remodeling complex. *Science*, **303**, 343–348.
21. Kobor, M. S., Venkatasubrahmanyam, S., Meneghini, M. D., Gin, J. W., Jennings, J. L., Link, A. J. *et al.* (2004). A protein complex containing the conserved Swi2/Snf2-related ATPase SWR1p deposits histone variant H2A.Z into euchromatin. *PLoS Biol.* **2**, E131.
22. Ikura, T., Ogryzko, V. V., Grigoriev, M., Groisman, R., Wang, J., Horikoshi, M. *et al.* (2000). Involvement of the TIP60 histone acetylase complex in DNA repair and apoptosis. *Cell*, **102**, 463–473.
23. Wood, M. A., McMahon, S. B. & Cole, M. D. (2000). An ATPase/helicase complex is an essential cofactor for oncogenic transformation by c-Myc. *Mol. Cell*, **5**, 321–330.
24. Matias, P. M., Gorynia, S., Donner, P. & Carrondo, M. A. (2006). Crystal structure of the human AAA^+ protein RuvBL1. *J. Biol. Chem.* **281**, 38918–38929.
25. Edgar, R. C. (2004). MUSCLE: a multiple sequence alignment method with reduced time and space complexity. *BMC Bioinformatics*, **5**, 113.
26. Edgar, R. C. (2004). MUSCLE: multiple sequence alignment with high accuracy and high throughput. *Nucleic Acids Res.* **32**, 1792–1797.
27. Neuwald, A. F., Aravind, L., Spouge, J. L. & Koonin, E. V. (1999). AAA^+: a class of chaperone-like ATPases associated with the assembly, operation, and disassembly of protein complexes. *Genome Res.* **9**, 27–43.
28. Makino, Y., Kanemaki, M., Kurokawa, Y., Koji, T. & Tamura, T. (1999). A rat RuvB-like protein, TIP49a, is a germ cell-enriched novel DNA helicase. *J. Biol. Chem.* **274**, 15329–15335.
29. Kocsis, E., Cerritelli, M. E., Trus, B. L., Cheng, N. & Steven, A. C. (1995). Improved methods for determination of rotational symmetries in macromolecules. *Ultramicroscopy*, **60**, 219–228.
30. Ksiezak-Reding, H. & Wall, J. S. (2005). Characterization of paired helical filaments by scanning transmission electron microscopy. *Microsc. Res. Tech.* **67**, 126–140.
31. Marrione, P. E. & Cox, M. M. (1996). Allosteric effects of RuvA protein, ATP, and DNA on RuvB protein-mediated ATP hydrolysis. *Biochemistry*, **35**, 11228–11238.
32. Tsaneva, I. R., Muller, B. & West, S. C. (1993). RuvA and RuvB proteins of *Escherichia coli* exhibit DNA helicase activity *in vitro*. *Proc. Natl Acad. Sci. USA*, **90**, 1315–1319.
33. Enemark, E. J. & Joshua-Tor, L. (2006). Mechanism of DNA translocation in a replicative hexameric helicase. *Nature*, **442**, 270–275.
34. Singleton, M. R., Sawaya, M. R., Ellenberger, T. & Wigley, D. B. (2000). Crystal structure of T7 gene 4 ring helicase indicates a mechanism for sequential hydrolysis of nucleotides. *Cell*, **101**, 589–600.
35. Ahnert, P. & Patel, S. S. (1997). Asymmetric interactions of hexameric bacteriophage T7 DNA helicase with the 5′- and 3′-tails of the forked DNA substrate. *J. Biol. Chem.* **272**, 32267–32273.
36. Delagoutte, E. & von Hippel, P. H. (2002). Helicase mechanisms and the coupling of helicases within macromolecular machines: Part I. Structures and properties of isolated helicases. *Q. Rev. Biophys.* **35**, 431–478.
37. Skordalakes, E. & Berger, J. M. (2006). Structural insights into RNA-dependent ring closure and ATPase activation by the Rho termination factor. *Cell*, **127**, 553–564.
38. Patel, S. S. & Picha, K. M. (2000). Structure and function of hexameric helicases. *Annu. Rev. Biochem.* **69**, 651–697.
39. Mitchell, A. H. & West, S. C. (1994). Hexameric rings

of *Escherichia coli* RuvB protein. Cooperative assembly, processivity and ATPase activity. *J. Mol. Biol.* **243**, 208–215.
40. Kuriyan, J. & O'Donnell, M. (1993). Sliding clamps of DNA polymerases. *J. Mol. Biol.* **234**, 915–925.
41. Zhang, X. D., Dou, S. X., Xie, P., Hu, J. S., Wang, P. Y. & Xi, X. G. (2006). *Escherichia coli* RecQ is a rapid, efficient, and monomeric helicase. *J. Biol. Chem.* **281**, 12655–12663.
42. Maluf, N. K., Fischer, C. J. & Lohman, T. M. (2003). A dimer of *Escherichia coli* UvrD is the active form of the helicase *in vitro*. *J. Mol. Biol.* **325**, 913–935.
43. Savchenko, A., Yee, A., Khachatryan, A., Skarina, T., Evdokimova, E., Pavlova, M. *et al.* (2003). Strategies for structural proteomics of prokaryotes: quantifying the advantages of studying orthologous proteins and of using both NMR and X-ray crystallography approaches. *Proteins: Struct. Funct. Genet.* **50**, 392–399.
44. Bradford, M. M. (1976). A rapid and sensitive method for the quantitation of microgram quantities of protein utilizing the principle of protein-dye binding. *Anal. Biochem.* **72**, 248–254.
45. Snider, J., Gutsche, I., Lin, M., Baby, S., Cox, B., Butland, G. *et al.* (2006). Formation of a distinctive complex between the inducible bacterial lysine decarboxylase and a novel AAA^+ ATPase. *J. Biol. Chem.* **281**, 1532–1546.
46. De Marco, V., Stier, G., Blandin, S. & de Marco, A. (2004). The solubility and stability of recombinant proteins are increased by their fusion to NusA. *Biochem. Biophys. Res. Commun.* **322**, 766–771.
47. Ludtke, S. J., Baldwin, P. R. & Chiu, W. (1999). EMAN: semiautomated software for high-resolution single-particle reconstructions. *J. Struct. Biol.* **128**, 82–97.
48. Chen, D. H., Song, J. L., Chuang, D. T., Chiu, W. & Ludtke, S. J. (2006). An expanded conformation of single-ring GroEL–GroES complex encapsulates an 86 kDa substrate. *Structure*, **14**, 1711–1722.
49. Frank, J. (2006). *Three Dimensional Electron Microscopy*, 2nd edition Oxford University Press, New York, NY; Chapter 2.
50. Hainfeld, J. F., Wall, J. S. & Desmond, E. J. (1982). A small computer system for micrograph analysis. *Ultramicroscopy*, **8**, 263–270.